Quantum Dot Biolabeling

DOI: 10.1002/anie.201202876

Conjugation of Transferrin to Azide-Modified CdSe/ZnS Core–Shell Quantum Dots using Cyclooctyne Click Chemistry**

Christine Schieber, Alessandra Bestetti, Jet Phey Lim, Anneke D. Ryan, Tich-Lam Nguyen, Robert Eldridge, Anthony R. White, Paul A. Gleeson, Paul S. Donnelly,* Spencer J. Williams,* and Paul Mulvaney**

Quantum dots (QDs) are semiconductor nanocrystals with unique optical properties that distinguish them from common organic fluorophores. For example, they give size-dependent emission spectra, high photoluminescence quantum yields, and large molar extinction coefficients, which gives the potential for single-molecule detection. They also have broad absorption cross-sections, which enables simultaneous excitation of mixed populations of QDs. Additionally, QDs are more resistant to chemical degradation and are less affected by photo-bleaching than conventional dyes.[1]

Many applications in diagnostics, biosensing, and biolabeling could benefit from the optical properties of QDs.[2] The first step of any method is the preparation of water soluble QDs, and various strategies have been developed to generate water-soluble nanoparticles.[3] The attachment of biomolecules such as proteins, monoclonal antibodies, or enzymes to water-soluble QDs is not trivial, and to date there is no generic conjugation method that is broadly applicable, easily implemented, and reproducible without compromising the function of the QDs.[4–6] Among the most powerful bioconjugation reactions to emerge are a set of bioorthogonal chemical reactions referred to as 'click' reactions. The copper(I)-catalyzed azide-terminal alkyne cycloaddition (CuAAC) reaction[7–9] provides exquisite functional-group selectivity and does not suffer the drawbacks of standard coupling reactions (for example, oxime/hydrazone ligation, esterification, and thiol-maleimide addition reactions) that are often susceptible to hydrolysis and/or cross-linking.[10] The CuAAC reaction has been extensively used for the functionalization of gold, silica, and iron oxide nanoparticles, as well as carbon nanotubes.[11–14] Unfortunately, addition of copper(I) to CdSe semiconductor QDs completely and irreversibly quenches QD photoluminescence (see Supporting Information).[15–17] An attractive alternative is the strain-promoted azide–alkyne cycloaddition (SPAAC) reaction of azides with strained cyclooctynes, which occurs rapidly and does not require a copper catalyst.[18,19]

Herein, we report a strategy to prepare azide-modified QDs using a previously reported QD polymer-encapsulation technique.[20] We have developed a modular and broadly applicable conjugation strategy based on a bifunctional linker (**L**) that enables incorporation of cyclooctyne groups onto the metalloprotein transferrin and the SPAAC conjugation of the cyclooctyne-modified transferrin to azide-modified QDs (Figure 1). Finally, we demonstrate that the QD–protein conjugates are biologically active by monitoring the uptake of fluorescent QD–transferrin conjugates in transferrin-receptor (TfR) expressing tumor cells.

CdSe/ZnS core–shell QDs were synthesized in octadecene using the SILAR (successive ion-layer adsorption reaction) process.[21] SILAR affords organic-soluble QDs with trioctylphosphine/trioctylphosphine oxide (TOP/TOPO) bound to the nanocrystal surface. Azide-modified water-soluble QDs were prepared from organic-soluble QDs in two steps (Figure 1 a). Treatment of the QDs with an excess of low molecular weight polystyrene-*co*-maleic anhydride polymer (PSMA, MW 1700) results in polymer encapsulation of the QD. Treatment of the PSMA-encapsulated QDs with a hydrophilic amino poly(ethylene glycol) (amino-PEG), Jeffamine M1000, results in aminolysis of the anhydride and spontaneous transfer to the aqueous phase. Controllable presentation of azide functional groups on the QD surface can be achieved by blending various amounts of an azide-modified $H_2N{-}PEG{-}N_3$ into Jeffamine M1000. The resulting PEG-modified polymer-encapsulated QDs were colloidally stable over a wide range of pH values and salt concentrations. Functionalization of QDs with PEG minimizes nonspecific binding to biological components, reduces cellular toxicity, and increases circulation times in vivo.[20,22–25] This phase-transfer method allows the QD surface to be derivatized with different functional groups in any desired ratio, and thus gives control over the number and density of biomolecules that will ultimately be attached. We denote the percentage of azide groups on the QDs as **QDx**, such that **QD0** corresponds to

[*] Dr. C. Schieber, A. Bestetti, A. D. Ryan, Dr. T.-L. Nguyen, R. Eldridge, Dr. P. S. Donnelly, Prof. S. J. Williams, Prof. P. Mulvaney
School of Chemistry and Bio21 Institute, University of Melbourne
Parkville, Vic 3010 (Australia)
E-mail: cschi@unimelb.edu.au
pauld@unimelb.edu.au
sjwill@unimelb.edu.au
mulvaney@unimelb.edu.au

Dr. J. P. Lim, Prof. P. A. Gleeson
Department of Biochemistry and Molecular Biology and Bio21 Institute, University of Melbourne
Parkville, Vic 3010 (Australia)

Dr. A. R. White
Department of Pathology, University of Melbourne
Parkville, Vic 3010 (Australia)

[**] This work was supported by the Faculty of Science, University of Melbourne, and the Australian Research Council (ARC).

Supporting information for this article (experimental details) is available on the WWW under http://dx.doi.org/10.1002/anie.201202876.

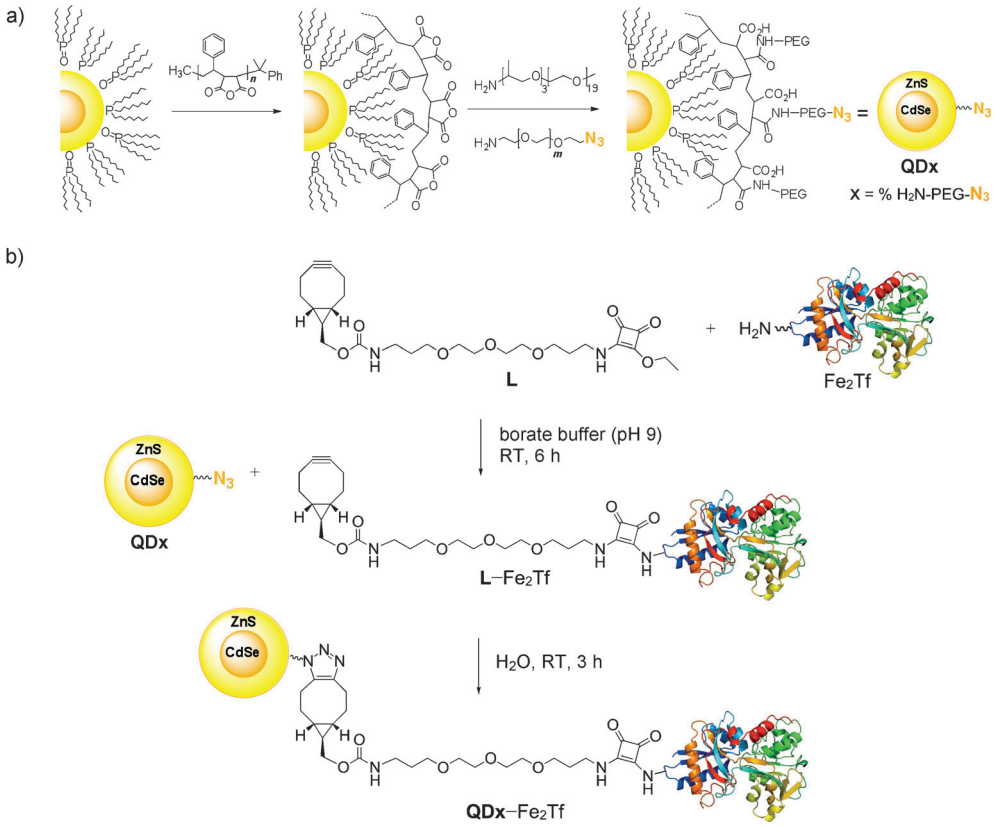

Figure 1. a) Polymer encapsulation of CdSe/ZnS core–shell nanoparticles. b) QD conjugation strategy: primary-amine coupling with ethyl squaramyl affords a squaramide conjugate between the linker **L** and Fe_2-transferrin (**L**-Fe_2Tf). Strain-promoted azide–alkyne cycloaddition of azide-modified QDs and **L**-Fe_2Tf yields QD-**L**-Fe_2Tf.

QDs without azide groups coated only with Jeffamine M1000, and **QD100** indicates QDs prepared using 100% H_2N–PEG–N_3.

The optical properties of the aqueous QDs were identical to those of the original QDs measured in organic solvents, indicating that no aggregation or surface degradation occurs upon polymer encapsulation and phase transfer (Figure 2a, left). The successful incorporation of azide groups was confirmed using FTIR spectroscopy by monitoring the characteristic azide absorption band ($\nu = 2100\ cm^{-1}$; Figure 2a, center). QDs were purified by size exclusion chromatography to remove residual PSMA (Figure 2a, right).

A bifunctional linker (**L**) bearing a cyclooctyne functional group and an electrophilic ethyl squaramate group was synthesized (see Supporting Information). Bicyclo-[6.1.0]nonyne (BCN) was chosen as the cyclooctyne because it is relatively simple to prepare, exhibits a high rate of reaction, and yields only one regioisomeric triazole product.[26] The ethyl squaramyl group[27] of **L** provides excellent shelf stability, yet reacts rapidly with amino groups to give proteins modified with pendent cyclooctynes, poised for reaction with azide-functionalized QDs.

This bioconjugation strategy was applied to the iron-binding glycoprotein transferrin (Fe_2Tf, MW = 80 kDa), which is involved in cellular iron-acquisition.[28] Upon *apo*-transferrin binding two Fe^{III} cations and a synergistic carbonate anion, iron-loaded transferrin (Fe_2Tf) binds to a transferrin receptor and is internalized into cells by way of clathrin-mediated endocytosis. Optimal conditions for the formation of **L**-Fe_2Tf were using a borate buffer (0.5 M, pH 9) incubated for six hours at room temperature.[27] The number of linker molecules bound to each Fe_2Tf was determined by ESI-TOF-MS when 2:1 (Figure 2b, center) and 4:1 (Figure S2) molar ratios of linker were added to the protein, with peaks observed corresponding to 0, 1, 2, or 3 linker molecules per protein. The reactivity of the cyclooctyne functional group was tested by reaction of **L**-Fe_2Tf with 2-azido-*N*-phenylacetamide (MW = 176 Da). A mass increase corresponding to addition of one or more molecules of the azide confirmed fast and efficient triazole formation (Figure 2b, bottom; and Figure S2).

To demonstrate that the azide groups on the azide-modified QDs are reactive to solution-phase cyclooctyne groups, the linker molecule **L** was reacted with Alexa Fluor 594 cadaverine (A594). The resulting **L**-A594 conjugate was reacted with QDs functionalized with different percentages of azide groups (**QD0**, **QD1**, **QD10**, **QD100**). Unreacted **L**-A594 was removed by exhaustive washing using spin filtration. Fluorescence spectra of QD-linker-dye samples upon excitation at 400 nm show FRET (Förster resonance energy transfer) between the QDs and the dye, with the FRET signal increasing with increasing azide loading on the QD (Figure 2c). This demonstrates a successful SPAAC reaction between the QDs and the linker and shows that the number of biomolecules attached to the QDs can be tuned by controlling the percentage of azide groups on the nanoparticle surface. A control reaction between **QD0** and **L**-A594 showed no FRET, indicating that the conjugate does not form and confirming the specificity of the SPAAC reaction.

Conjugation of QDs with transferrin was achieved by first reacting Fe_2Tf with the linker **L**, and then the resulting **L**-Fe_2Tf conjugate was added in tenfold excess to **QD0**, **QD10**, and **QD100**. Samples were analyzed by gel electrophoresis (Figure 2d). Because the QD surface is negatively charged, all samples migrated from the negative to the positive pole and their speed was determined by their charge and size. For increasing density of azide groups on the QD surface, the

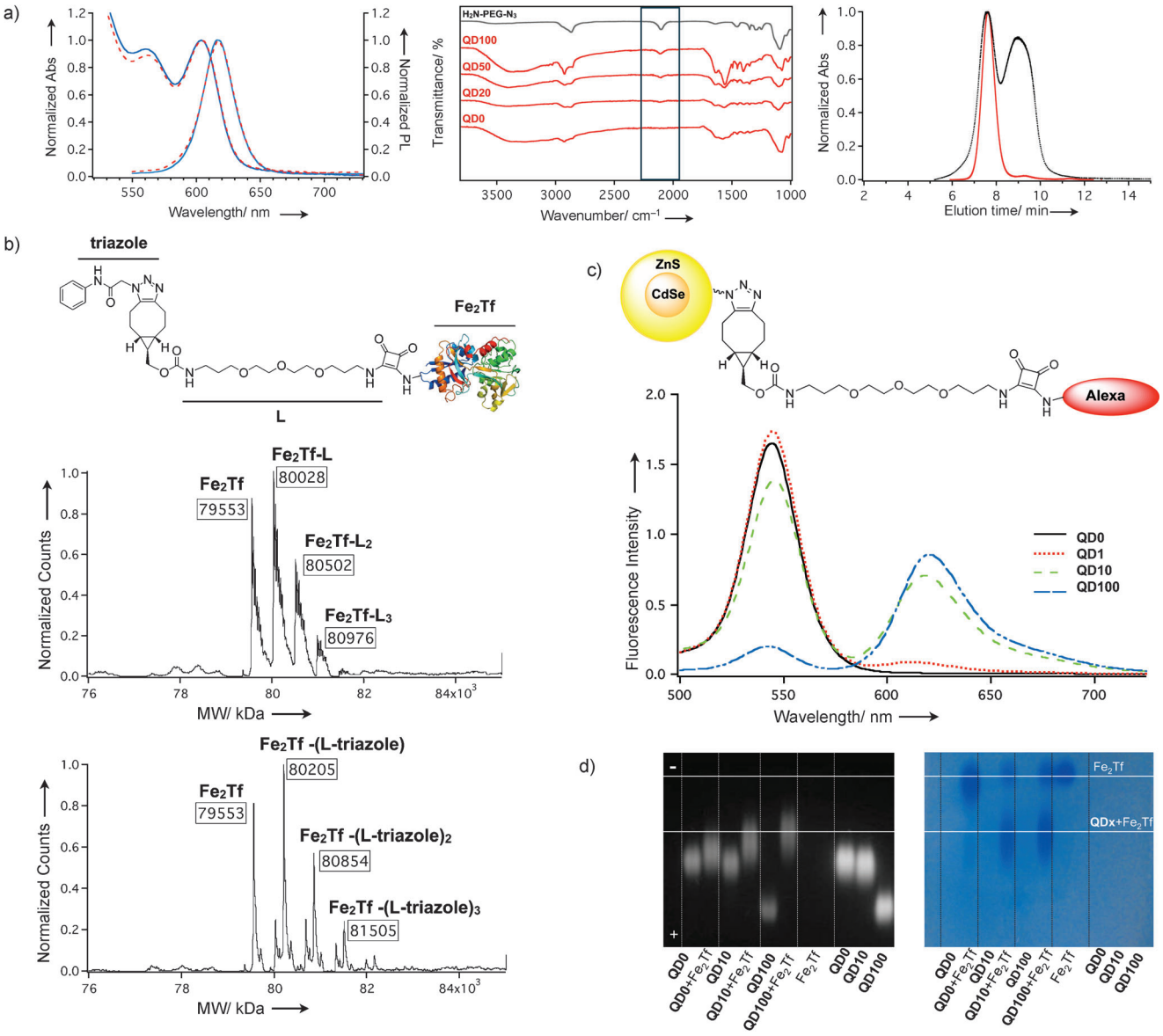

Figure 2. a) Left: Absorption and emission spectra before (red) and after (blue) $CHCl_3$/water phase transfer of QDs. Center: Comparison of FTIR spectra of H_2N–PEG–N_3 and QDs functionalized with 0–100% azide groups. Right: Size-exclusion chromatogram of a crude QD sample (black) and of the same sample after purification (red) measured at 220 nm. b) Top: Chemical formula of the triazole-conjugated Fe_2Tf. Center: ESI-TOF MS of **L**-Fe_2Tf formed by treatment of Fe_2Tf with linker (**L**) at a 2:1 ratio. The difference in mass between the peaks is 475 Da (476 Da calculated). Bottom: Reaction of azidophenylacetamide at a 1:1 ratio with the 2:1 complex of **L**-Fe_2Tf. c) Fluorescence spectra of **QDx** + L-A594 collected after removal of excess dye. QDs emit at 543 nm and Alexa Fluor 594 emits at 617 nm. d) Agarose gel electrophoresis of QDs and **QDx** + Fe_2Tf under UV lamp (left) and after staining with Coomassie blue (right).

difference in mobility between unconjugated and conjugated samples increased. Because Fe_2Tf has a pI of 5.2–6.2[29] and is negatively charged at the basic pH used for gel electrophoresis, the reduced mobility of the **QDx**-Fe_2Tf samples can thus be ascribed to an increase in the hydrodynamic volume, which indicates the success of the conjugation between QDs and **L**-Fe_2Tf. Also, only the **QD10**-Fe_2Tf and **QD100**-Fe_2Tf conjugates are stained by Coomassie blue, indicating the presence of conjugated protein, whereas for **QD0** and Fe_2Tf, the Coomassie stain appears only at the position of the free protein.

QDx-Fe_2Tf conjugates were also characterized by analytical ultracentrifugation, which allows determination of the hydrodynamic diameter and MW of a particle from its sedimentation behavior. The samples showed a trend towards higher sedimentation coefficients with increasing percentages of azide, in agreement with the results from gel electrophoresis (Supporting Information, Figure S3), and confirmed the specificity of the conjugation strategy, as well as the success of the purification.

The uptake of **QD100**-Fe_2Tf conjugates into HeLa cells was studied to demonstrate that the conjugates retained biological activity, relative to Alexa Fluor 568 (A568)-labeled Fe_2Tf. HeLa cells express TfRs and following uptake, Fe_2Tf is trafficked to the early endosomes. Following release of the iron atoms, *apo*-Tf is recycled to the plasma membrane. These

studies involved binding of Fe_2Tf to cell-surface TfRs with the cells on ice to retard endocytosis. Unbound Fe_2Tf was washed off the cells and internalization of the receptor-bound Fe_2Tf was initiated by warming the cells to 37 °C. Both A568-Fe_2Tf and **QD100**-Fe_2Tf conjugates were internalized into HeLa cells within 15-30 minutes (Figure 3). Control experiments with unconjugated **QD100** demonstrated that the binding was Fe_2Tf-dependent (Figure 3, C1–3). Together these results strongly suggest that **QD100**-Fe_2Tf binds to the TfR and is internalized by receptor-mediated endocytosis. After incubation at 37 °C for 30 minutes, both the amount of uptake and the intracellular distribution of **QD100**-Fe_2Tf and A568-Fe_2Tf were similar. However, two hours after treatment, cells incubated with A568-Fe_2Tf had significantly reduced intracellular fluorescence than at 30 minutes, indicating that the conjugate is trafficked out of the cell by known Fe_2Tf cellular-efflux pathways (Figure 3, A2 and A3). In contrast, at two hours in cells treated with **QD100**-Fe_2Tf, significant punctate staining remained (Figure 3, B3), demonstrating that A568-Fe_2Tf and **QD100**-Fe_2Tf have different rates of efflux.

To further investigate the localization of **QD100**-Fe_2Tf after internalization, cells were stained for markers of endocytic compartments. Early endosome antigen 1 (EEA1) is a marker for early endosomes and CD63 for late endosomes/lysosomes. After 15 minutes, **QD100**-Fe_2Tf showed extensive co-localization with EEA1 but minimal co-localization with CD63 (Figure 4a). Conversely, after two hours, **QD100**-Fe_2Tf showed significant overlap with the lysosomal marker CD63 (Figure 4b). These results demonstrate successful binding of **QD100**-Fe_2Tf to TfRs and internalization into cells, although the presence of the QDs appears to

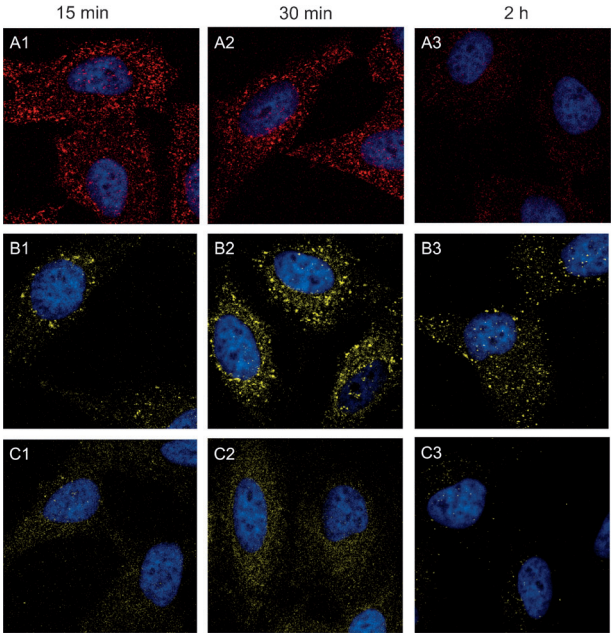

Figure 3. Fe_2-transferrin uptake into HeLa cells using A568-Fe_2Tf (A1–A3), **QD100**-Fe_2Tf (B1–B3), and **QD100** (C1–C3) for the indicated times at 37 °C. Cells were fixed in 4% paraformaldehyde and nuclei stained with DAPI. Images of **QD100**-Fe_2Tf and the corresponding unconjugated **QD100** control were taken at the same gain setting.

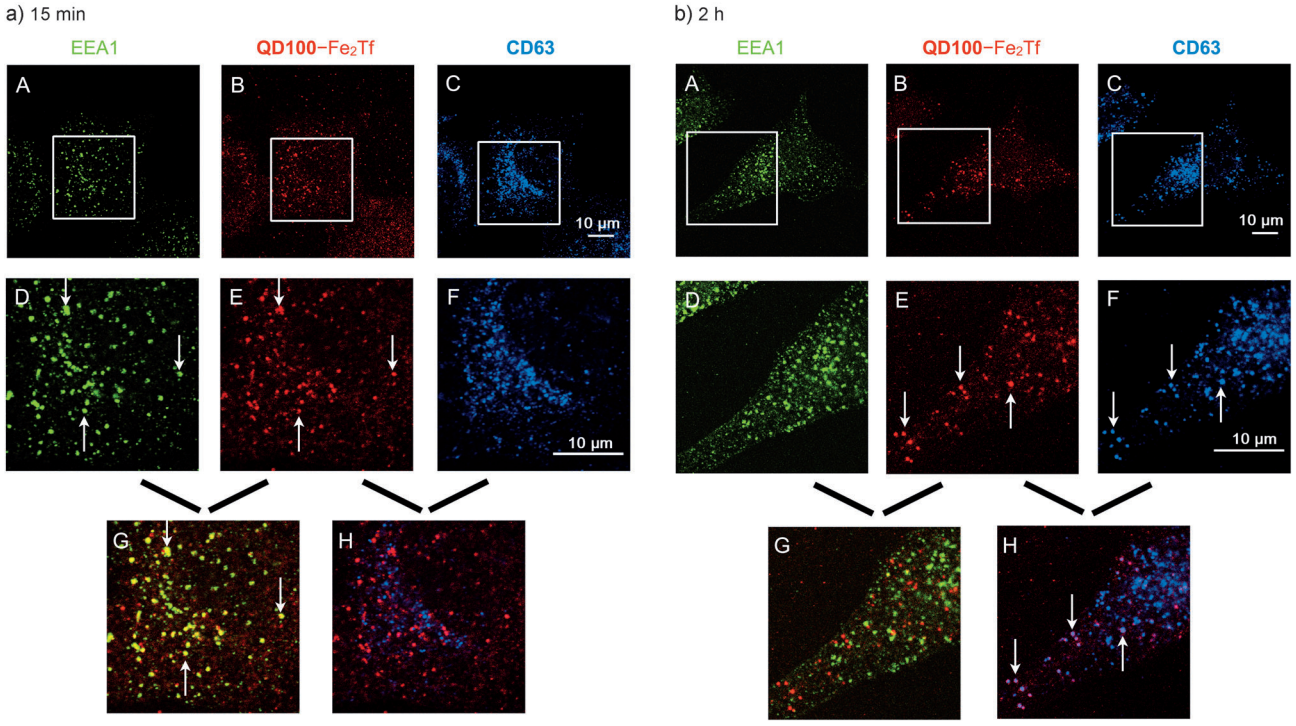

Figure 4. a) **QD100**-Fe_2Tf uptake into HeLa cells were performed for 15 min at 37 °C. Cells were fixed in 4% paraformaldehyde and stained with rabbit anti-EEA1 followed by A568-conjugated anti-rabbit IgG, and mouse anti-CD63 followed by A647-conjugated anti-mouse IgG. A, D) EEA1 (green); B, E) **QD100**-Fe_2Tf (red); C, F) CD63 (blue). D–H) 2× magnification of the boxed region. G) overlay of (D–E); H) overlay of (E–F). Co-localization is indicated by: yellow = **QD100**-Fe_2Tf + EEA1; magenta = **QD100**-Fe_2Tf + CD63. b) **QD100**-Fe_2Tf uptake into HeLa cells was performed for 2 h at 37 °C. All colors and procedures are the same as in (a). Representative regions of overlap are indicated by arrows.

perturb the intracellular trafficking pathway compared to Alexa Fluor-labeled Fe_2Tf, resulting in retarded efflux. This last observation is consistent with reports by others using Fe_2Tf-QD conjugates in HeLa, HEp-2, and SW480 cells, despite using entirely different conjugation strategies to generate the protein–QD conjugates.[30–32]

In summary, we reported a method for the production and analysis of biocompatible, water-soluble, protein-conjugated QDs. The surface modification strategy used herein allows for control of the proportion of azide groups on the surface of the QD and can be extended to other functional groups simply by varying the amino-PEG reagent. The azide-modified QDs undergo specific and efficient bioconjugation to a protein modified with a bifunctional linker, containing a squaramate for reaction with amines and a symmetrical cyclooctyne that undergoes SPAAC with QD-displayed azide groups. Interestingly, the biological function of Fe_2Tf was retained; however, differences were noted in the trafficking of QD-conjugated Fe_2Tf versus an organic dye. This method allows for control over a range of aspects of QD synthesis and conjugation, uses an easily synthesized bioconjugation reagent with a long shelf-life that retains protein function, and maintains the high fluorescence quantum yields and colloidal stability of the QDs.

Received: April 15, 2012
Revised: July 5, 2012
Published online: September 20, 2012

Keywords: bioconjugation · click chemistry · imaging · quantum dots · transferrin

[1] U. Resch-Genger, M. Grabolle, S. Cavaliere-Jaricot, R. Nitschke, T. Nann, *Nat. Methods* **2008**, *5*, 763 – 775.
[2] I. L. Medintz, H. T. Uyeda, E. R. Goldman, H. Mattoussi, *Nat. Mater.* **2005**, *4*, 435 – 446.
[3] F. Zhang, E. Lees, F. Amin, P. Rivera-Gil, F. Yang, P. Mulvaney, W. J. Parak, *Small* **2011**, *7*, 3113 – 3127.
[4] W. R. Algar, D. E. Prasuhn, M. H. Stewart, T. L. Jennings, J. B. Blanco-Canosa, P. E. Dawson, I. L. Medintz, *Bioconjugate Chem.* **2011**, *22*, 825 – 858.
[5] J. B. Delehanty, H. Mattoussi, I. L. Medintz, *Anal. Bioanal. Chem.* **2009**, *393*, 1091 – 1105.
[6] V. Biju, T. Itoh, M. Ishikawa, *Chem. Soc. Rev.* **2010**, *39*, 3031 – 3056.
[7] J. E. Hein, V. V. Fokin, *Chem. Soc. Rev.* **2010**, *39*, 1302 – 1315.
[8] C. W. Tornøe, C. Christensen, M. Meldal, *J. Org. Chem.* **2002**, *67*, 3057 – 3064.
[9] V. V. Rostovtsev, L. G. Green, V. V. Fokin, K. B. Sharpless, *Angew. Chem.* **2002**, *114*, 2708 – 2711; *Angew. Chem. Int. Ed.* **2002**, *41*, 2596 – 2599.
[10] E. Lallana, E. Fernandez-Megia, R. Riguera, *J. Am. Chem. Soc.* **2009**, *131*, 5748 – 5750.
[11] N. Li, W. H. Binder, *J. Mater. Chem.* **2011**, *21*, 16717 – 16734.
[12] E. Boisselier, L. Salmon, J. Ruiz, D. Astruc, *Chem. Commun.* **2008**, 5788 – 5790.
[13] L. Nebhani, C. Barner-Kowollik, *Adv. Mater.* **2009**, *21*, 3442 – 3468.
[14] G. von Maltzahn, Y. Ren, J.-H. Park, D.-H. Min, V. R. Kotamraju, J. Jayakumar, V. Fogal, M. J. Sailor, E. Ruoslahti, S. N. Bhatia, *Bioconjugate Chem.* **2008**, *19*, 1570 – 1578.
[15] W. H. Binder, R. Sachsenhofer, C. J. Straif, R. Zirbs, *J. Mater. Chem.* **2007**, *17*, 2125 – 2132.
[16] A. Bernardin, A. Cazet, L. Guyon, P. Delannoy, F. Vinet, D. Bonnaffé, I. Texier, *Bioconjugate Chem.* **2010**, *21*, 583 – 588.
[17] H.-S. Han, N. K. Devaraj, J. Lee, S. A. Hilderbrand, R. Weissleder, M. G. Bawendi, *J. Am. Chem. Soc.* **2010**, *132*, 7838 – 7839.
[18] N. J. Agard, J. A. Prescher, C. R. Bertozzi, *J. Am. Chem. Soc.* **2004**, *126*, 15046 – 15047.
[19] E. M. Sletten, C. R. Bertozzi, *Angew. Chem.* **2009**, *121*, 7108 – 7133; *Angew. Chem. Int. Ed.* **2009**, *48*, 6974 – 6998.
[20] E. Lees, T. Nguyen, A. Clayton, P. Mulvaney, *ACS Nano* **2009**, *3*, 1121 – 1128.
[21] J. van Embden, P. Mulvaney, *Langmuir* **2005**, *21*, 10226 – 10233.
[22] E. Chang, W. W. Yu, V. L. Colvin, R. Drezek, *J. Biomed. Nanotechnol.* **2005**, *1*, 397 – 401.
[23] K. Susumu, H. T. Uyeda, I. L. Medintz, T. Pons, J. B. Delehanty, H. Mattoussi, *J. Am. Chem. Soc.* **2007**, *129*, 13987 – 13996.
[24] W. Liu, M. Howarth, A. B. Greytak, Y. Zheng, D. G. Nocera, A. Y. Ting, M. G. Bawendi, *J. Am. Chem. Soc.* **2008**, *130*, 1274 – 1284.
[25] A. S. Karakoti, S. Das, S. Thevuthasan, S. Seal, *Angew. Chem.* **2011**, *123*, 2024 – 2040; *Angew. Chem. Int. Ed.* **2011**, *50*, 1980 – 1994.
[26] J. Dommerholt, S. Schmidt, R. Temming, L. J. A. Hendriks, F. P. J. T. Rutjes, J. C. M. van Hest, D. J. Lefeber, P. Friedl, F. L. van Delft, *Angew. Chem.* **2010**, *122*, 9612 – 9615; *Angew. Chem. Int. Ed.* **2010**, *49*, 9422 – 9425.
[27] S.-J. Hou, R. Saksena, P. Kovác, *Carbohydr. Res.* **2008**, *343*, 196 – 210.
[28] H. Sun, H. Li, P. J. Sadler, *Chem. Rev.* **1999**, *99*, 2817 – 2842.
[29] P. Grange, M. Mouricout, *Infect. Immun.* **1996**, *64*, 606 – 610.
[30] C. Tekle, B. V. Deurs, K. Sandvig, T.-G. Iversen, *Nano Lett.* **2008**, *8*, 1858 – 1865.
[31] T.-G. Iversen, N. Frerker, K. Sandvig, *Proc. SPIE-Int. Soc. Opt. Eng.* **2009**, *7189*, 71890T/71891 – 71890T/71899.
[32] W. C. Chan, S. Nie, *Science* **1998**, *281*, 2016 – 2018.

